IEEE Access
Multidisciplinary | Rapid Review | Open Access Journal

Received 28 November 2022, accepted 13 December 2022, date of publication 19 December 2022,
date of current version 29 December 2022.

Digital Object Identifier 10.1109/ACCESS.2022.3230715

RESEARCH ARTICLE

Optimal Braking Torque Distribution of Dual-Motor Front-Rear Individually Driven Electric-Hydraulic Hybrid Powertrain Based on Minimal Energy Loss

CHANG LUO[1], YANG YANG[1,2], (Member, IEEE), AND ZHEN ZHONG[1]
[1]State Key Laboratory of Mechanical Transmissions, Chongqing University, Chongqing 400444, China
[2]College of Mechanical and Vehicle Engineering, Chongqing University, Chongqing 400444, China

Corresponding author: Yang Yang (yangyang@cqu.edu.cn)

This work was supported in part by the National Natural Science Foundation of China under Grant 51575063, in part by the National Key Research and Development Program of China under Grant 2018YFB0106100, and in part by the State Key Laboratory of Mechanical Transmissions of Chongqing University, China.

ABSTRACT Regenerative braking is one of the most important methods for improving energy utilization in electric vehicles. Electric vehicles with front-rear, individually driven configurations exhibit significant potential and flexibility for recovering braking energy. To improve the system's high-power impact tolerance, a high-power density hydraulic energy storage system can be incorporated to facilitate a full-drive dual-motor electric–hydraulic hybrid (DMEHH) powertrain. The DMEHH system is composed of an independently driven electric–hydraulic hybrid front axle and a purely electric rear axle. In this study, a method for distributing braking torque to minimize energy loss was devised based on the proposed DMEHH powertrain. Power loss models for both the electric and hydraulic subsystems have been developed. Loss minimization control was adapted for the power loss model of the permanent magnet synchronous motors in the powertrain, and the front-rear and front electric–hydraulic torque braking distribution maps were calculated using the energy-loss minimization rule. The application of torque distribution maps resulted in energy losses less than those of the general ideal torque distribution for all braking conditions. The energy loss decreased by 27.2% when the loss minimization control method was used in the WLTC cycle, and decreased by 29.1%, 25.5%, and 21.6% in UDDS, NEDC, and US06 driving cycles, respectively.

INDEX TERMS Dual-motor individually driven powertrain, electric–hydraulic hybrid system, energy loss minimization, regenerative braking, torque distribution.

I. INTRODUCTION

The automotive industry has increasingly focused on electrically powered vehicles to alleviate the increasing energy and environmental crises being experienced around the world [1]. To reduce gasoline consumption and improve energy usage in electric vehicles, fossil fuel-powered systems can partially or completely be replaced by electrical power systems [2]. Furthermore, electric motors are versatile and can be installed in numerous arrangements and orientations. They can be installed on either the front or rear axles [3]. To achieve greater flexibility, precise torque control, higher load rate, and greater energy recovery, an electric motor can be installed on each axle of a dual-motor-driven electric vehicle [3], [4], [5].

One method to increase the energy utilization efficiency of an electric vehicle is braking energy recycling, which uses the four-quadrant characteristic of an electric motor [6]. Gao et al. [6] discussed three braking distributions: ideal front-rear braking distribution, optimal energy recovery braking, and parallel braking, which

The associate editor coordinating the review of this manuscript and approving it for publication was N. Prabaharan.

served as a basis for subsequent regenerative braking studies.

As the braking torque can be adjusted between the front and rear axles to adapt to changes in the front-rear braking force distribution, dual-motor, or front-rear-driven electric vehicles can achieve a higher energy recycling rate [7]. The power distribution between the front and rear power sources is one of the main aspects of dual-motor-driven electric vehicles. Kim [8] and Yuan et al. [9] optimized the power distribution of a four-wheel-drive electric powertrain based on the efficiency maps of the front and rear motors. The efficiency map varied based on the underlying current control [10]. In most cases, the zero-d-axis control or maximum torque per ampere (MPTA) control method is used [11]. However, when compared to these two control methods, loss minimization control (LMC), whose goal is to minimize the loss of the electric motor, exhibits a lower energy loss [12], [13], [14]. In this study, the LMC was used on electric motors to minimize the energy loss of the entire dual-motor-driven electric powertrain.

Because of its high power density, a hydraulic propulsion system performs well when used for regenerative braking, particularly under high-intensity start/stop conditions [15]. To reduce the use of fuel, hydraulic propulsion systems have been incorporated into conventional fossil-fuel vehicles [16]. For example, PSA Peugeot Citroën unveiled a type of hydraulic hybrid powertrain for passenger cars known as a hybrid air system, which has been proven to produce lower emissions than gasoline powertrains alone [17].

Owing to the operating mechanism of an electric battery, when a vehicle is braked at high deceleration or started at high acceleration, overloaded charging or discharging currents can adversely affect the health of the battery [18], [19]. This disadvantage can be mitigated by introducing a high power–density hydraulic energy conversion and reserve system [20]. An electric drive system combined with a hydraulic energy reserve system, also known as an electric–hydraulic hybrid system, can further improve the braking energy utilization efficiency [21], [22], [23].

The advantages of getting the hydraulic regenerative braking system involved in electric vehicles were also demonstrated in [24] by the authors. In the previous work, two different energy management strategies, maximum energy recovery and minimum current impact, are investigated. The results showed that by introducing the hydraulic energy storage system both strategies can reduce the charge currents during the vehicle's braking process.

In this study, a dual-motor-driven electric-hydraulic hybrid (DMEHH) powertrain, which integrates the advantages of the front-rear independently driven powertrain and hydraulic propulsion system, is proposed. Power loss models for the electric and hydraulic subsystems were established to minimize the energy loss of the entire DMEHH powertrain. The target function, which is an energy loss function with independent variables of the torque distribution coefficients, was established based on these models. The optimal torque distribution scheme was determined by minimizing the target function under certain constraints.

II. SYSTEM CONFIGURATION

The proposed DMEHH powertrain is a front-rear individually driven powertrain equipped with an electric–hydraulic hybrid energy storage system on the front axle. The front axle of the DMEHH system is operated by both the electric motor and hydraulic pump/motor (also known as the ''secondary element''), whereas the rear axle is operated solely by the electric motor, as shown in Fig. 1.

When the vehicle is braking, three different subsystems must be considered; the electric energy storage, hydraulic energy storage, and frictional brake subsystems. The electric energy storage subsystem includes front and rear electric motors (and their inverters) and a battery. Motors are primary energy conversion components that convert electric energy into mechanical energy to either operate the vehicle or recover kinetic energy when the vehicle is required to brake. The hydraulic subsystem includes two accumulators (high pressure and low pressure), a valve block, and a hydraulic pump/motor. The output shaft of the hydraulic pump/motor was connected directly to the shaft of the front electric motor by a clutch. When the clutch is engaged in braking mode, the hydraulic pump pumps hydraulic oil from the low-pressure accumulator to the high-pressure accumulator, generating braking torque and absorbing braking energy. The recovered energy is then stored, as excess pressure, in the high-pressure accumulator. While driving, the pressure in the high-pressure accumulator is released and drives the hydraulic pump/motor, which operates as a motor and provides driving torque. The valve block controls the direction of the oil flow using a controller. The conventional frictional subsystem is essential for braking safety and can compensate for the braking force when the required braking force exceeds the force provided by the regenerative braking systems.

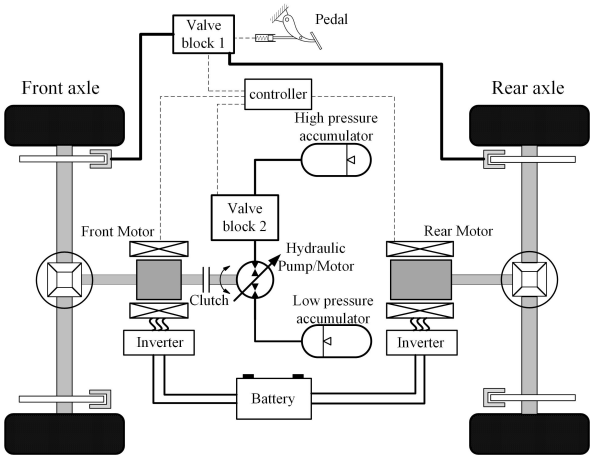

FIGURE 1. System structure of the DMEHH powertrain.

Depending on the energy management strategy used for a vehicle, the required braking torque can be provided and

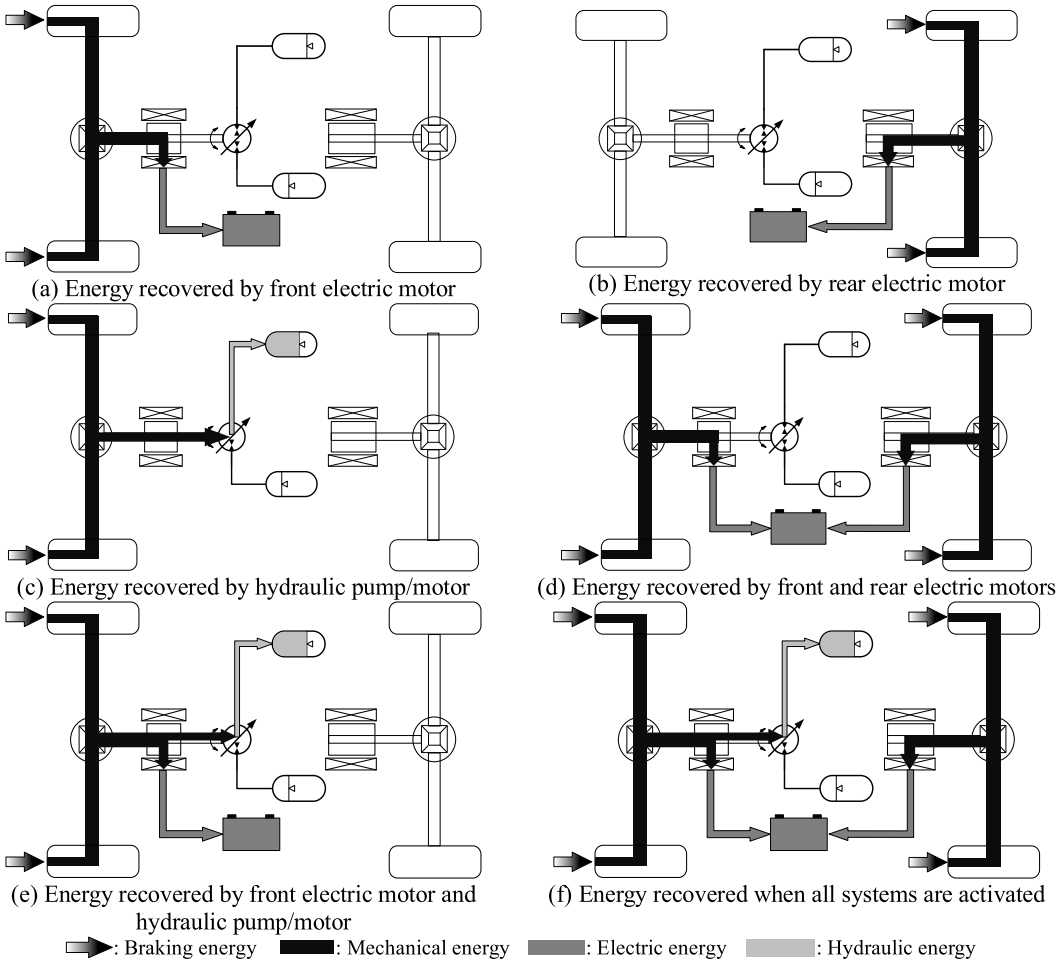

FIGURE 2. Energy flow pattern in different regenerative braking modes.

adjusted individually by controlling the front and rear motors or by adjusting the hydraulic pump/motor, resulting in various braking modes, which generate different energy flow paths when the braking energy is recovered. Fig. 2(a), (b), and (c) show the energy flow paths of the recovered braking energy when the braking energy is recovered by the front electric motor, rear electric motor, and hydraulic pump/motor, respectively. Fig. 2(d) and (e) show the energy flow paths when both the front and rear electric motors are activated and when both the front electric motor and the hydraulic pump/motor are activated, respectively. Finally, Fig. 2(e) shows the energy flow path when all the energy recovery systems are activated. Because various braking modes can achieve equal braking torques, the energy recovery efficiencies vary depending on the different characteristics of the energy conversion and storage elements.

Table 1 shows the parameters of the main components of the DMEHH.

III. MATHEMATICAL MODELING

The sum of the energy dissipated during braking is the objective function of the energy-loss minimization problem. The DMEHH powertrain is comprised of two distinct subsystems; an electric power subsystem and a hydraulic power subsystem. Additionally, the friction braking system must be considered when a vehicle brakes, and because the friction system cannot recover any braking energy, it is modeled as a simple braking torque. The electric subsystem comprises two motors, two inverters, and a battery pack, whereas the hydraulic subsystem comprises a hydraulic pump/motor, a set of electric control hydraulic valves, and two accumulators, and each of these components requires its own energy loss model.

A. PERMANENT MAGNET SYNCHRONOUS MOTOR (PMSM) LOSS MINIMIZATION CONTROL MODEL

The PMSM is a critical component of the DMEHH powertrain. During driving, it converts electrical energy into mechanical energy, and during braking, it converts mechanical energy into electrical energy. When a PMSM is operating, four types of power losses occur: copper, iron, mechanical, and stray losses [3]. The stray loss was disregarded in our study because of its small magnitude compared

TABLE 1. Specifications of the DMEHH vehicle.

Vehicle	Total vehicle mass (kg)	1870
	Wheel radius (m)	0.36
	Gravity center height (m)	0.56
	Wheel base (m)	2.7
	Distance from gravity center to front wheel center (m)	1.2
	Rolling resistance coefficient	0.015
	Drag coefficient	0.4
	Ratio of front final drive	5.35
	Ratio of rear final drive	4.8
Front motor	Rated/peak power (kW)	35/75
	Rated/peak torque (Nm)	111/239
	Rated/peak rotation speed (rpm)	3000/7000
Rear motor	Rated/peak power (kW)	50/107
	Rated/peak torque (Nm)	160/350
	Rated/peak rotation speed (rpm)	3000/6000
Hydraulic system	Accumulator volume (L)	10
	Max/min pressure (MPa)	33/16
	Max displacement (mL/r)	28
	Max rotation speed (rpm)	6300

to that of the others. The mechanical loss of the PMSM is assumed to be independent of the torque so that it is not affected by the torque distribution strategy [5]. Hence, the stray loss will be ignored and the mechanical loss will be included when establishing the loss model of the PMSM.

A PMSM is typically driven by a three-phase alternating current. By introducing direct and quadrature-axis transformations, the stator quantities are transformed into equivalent quantities that rotate synchronously with the rotor. Under steady-state conditions, the interactions between the stator and rotor magnetomotive force (MMF) (or flux waves) become those of a constant MMF, separated by a constant spatial angle. Hence, the PMSM model can be represented as two equivalent circuits [12].

Considering the iron and copper losses, the d-axis and q-axis equivalent circuit models of a PMSM are shown in Fig. 3. The equivalent iron loss resistances are connected in parallel in the circuits, whereas the copper loss resistances are connected in series. The d-axis and q-axis currents (i_d and i_q) are divided into the iron loss current (i_{cd} and i_{cq}) and the torque current (i_{od} and i_{oq}). The d-axis and q-axis equivalent back EMFs are presented by the voltage sources $-\omega_e L_q i_{oq}$ and $\omega_e (L_d i_{od} + \psi_{PM})$.

Various current control methods, such as MPTA control, $i_d = 0$ control, and LMC, can be used to achieve equal output torque in PMSMs [11]. The LMC method was adopted for PMSM control since the goal of this study is to minimize energy loss during vehicle braking. The LMC method is summarized as follows [25].

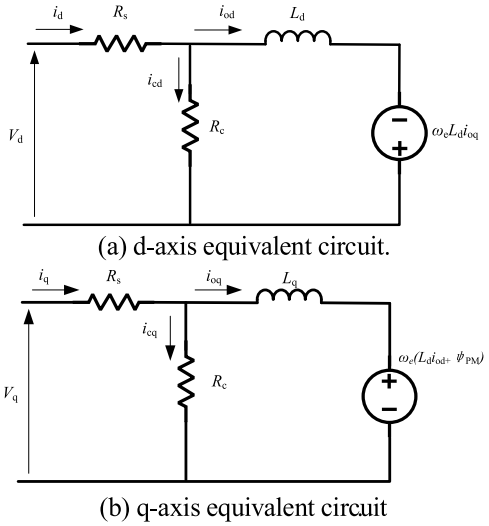

FIGURE 3. D- and q-axis equivalent circuit models of PMSM for power loss.

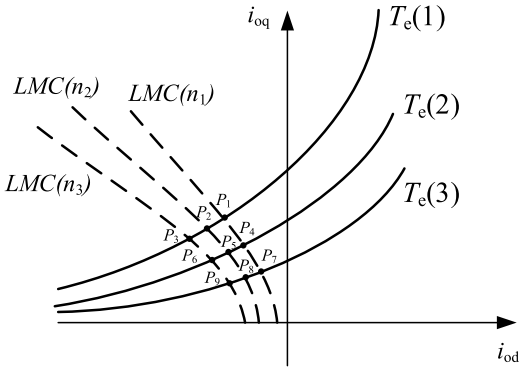

FIGURE 4. FIGURE 4. LMC trajectory family and torque trajectory in i_{od}–i_{oq} plane.

The copper and iron loss powers can be written as [13]

$$P_{Cu} = \frac{3}{2} R_c \left[\left(i_{od} - \frac{\omega_e L_q i_{oq}}{R_c} \right)^2 + \left(i_{oq} + \frac{\omega_e L_d i_{od} + \omega_e \psi_{PM}}{R_c} \right)^2 \right]$$

$$P_{iron} = \frac{3}{2} \left[\frac{\omega_e^2 L_q^2 i_{oq}^2}{R_c} + \frac{\omega_e^2 (\psi_{PM} + L_d i_{od})^2}{R_c} \right] \quad (1)$$

where L_d and L_q are the d-axis and q-axis inductances, respectively; R_s is the winding resistance; R_c is the iron loss resistance, ψ_{PM} is the permanent magnet flux linkage; and ω_e is the electrical frequency in radians, which is expressed as $\omega_e = (poles/2)\,\omega_m$ in terms of the mechanical frequency ω_m.

Hence, the total electromagnetic loss of the electric motor, P_{loss_mtr}, can be written as a function of the electrical rotational speed ω_e and torque currents i_{od} and i_{oq} as follows:

$$P_{loss\_mtr} = P_{Cu} + P_{iron} = P(i_{od}, i_{oq}, \omega_e) \quad (2)$$

It can be seen that the power loss of the PMSM is a function of variables i_{od}, i_{oq}, and ω_e. To obtain the values of i_{od} and i_{oq} which minimize the power loss in different working conditions, a quasi-static-state condition is preset for the PMSM. This implies that the electromagnetic torque and the rotational speed of the PMSM are steady.

The electromagnetic torque of the PMSM is expressed as

$$T_e = \frac{3}{2}\frac{Poles}{2}\left[\psi_{PM} i_{oq} + (L_d - L_q) i_{od} i_{oq}\right] \tag{3}$$

Based on this torque equation, the q- part of the current i_{oq} can be expressed as a function of i_{od} and T_e, shown as

$$i_{oq} = \frac{4T_e}{poles\left[\psi_{PM} + (L_d - L_q) i_{od}\right]} \tag{4}$$

By substituting (4) into the power loss equation (2), the power loss of the PMSM becomes a function of variables $i_{od,}$, T_e and ω_e, The quasi-static-state condition reduces the independent variables of the power loss function to one: i_{od}. To obtain the point for the power loss minimization, the derivative of P_{total_mtr} with respect to i_{od} should be set to zero, as follows:

$$\frac{\partial P_{loss\_mtr}}{\partial i_{od}} = 0 \tag{5}$$

By solving this partial differential equation, the value of i_{od} when the PMSM's power loss is at its minimum. The value of i_{oq} can be calculated by (4). Hence, the values of d- and q-part of the torque current i_{od} and i_{oq} which make the PMSM's power loss reach its minimum can be calculated, as well as the minimum value of the power loss. By taking different steady-state values of T_e and ω_e, the corresponding minimized power loss can be obtained. Therefore, the power loss of the PMSM which uses LMC control can be expressed as a function of electromagnetic torque T_e and rotational speed ω_m (ω_m is proportional to ω_e by factor *Poles*/2).

Another method can be presented to briefly illustrate that the power loss of the PMSM with the LMC control strategy is a function of T_e and ω_m. Considering the electromagnetic torque's quasi-static state, the change rate of T_e equals zero, which can be expressed as

$$\frac{\partial T_{total}}{\partial i_{od}} = 0 \tag{6}$$

Combining (5) and (6), a quadratic equation of i_{od} and i_{oq} with ω_m as a parameter in its coefficients will be generated. The curves series which rely on rotational speed can be drawn in the i_{od}-i_{oq} plane (dotted lines in Fig. 4). These trajectories show relationships of i_{od} and i_{oq} of the PMSM under LMC control strategy in different rotational speeds. By drawing the torque contour (determined by equation 3) in the i_{od}-i_{oq} plane, it can be noticed that the intersection points represent the values of current pairs (i_{od}, i_{oq}) under the LMC control strategy of the PMSM (Points P_1—P_9 shown in Fig. 4 as demonstrations).

By transforming the coordinates from i_{od}-i_{oq} to T_e-ω_m, the power loss of the PMSM, P_{loss_mtr}, can be expressed as a function of the output torque T_e and rotational speed ω_m, which is:

$$P_{loss\_mtr} = P_{loss\_mtr}(T_e, \omega_m) \tag{7}$$

B. INVERTER POWER LOSS MODEL

The inverter converts direct current into alternating current to control the output torque of the PMSM via space-vector pulse modulation by switching insulated gate bipolar transistors (IGBTs). IGBT losses can be classified into two categories: conduction and switching losses. A three-phase PMSM requires a three-phase full-bridge inverter with six IGBTs and six diodes connected in an anti-parallel manner [26]. Hence, the total inverter loss can be expressed as follows:

$$\begin{aligned} P_{loss\_inv} = {} & 6K_1 I_{peak} + 6K_2 I_{peak}^2 \\ & + 6K_3 \frac{m}{4} I_{peak} \cos\varphi + 6K_4 \frac{m}{3\pi} I_{peak}^2 \cos\varphi \end{aligned} \tag{8}$$

where I_{peak} is the amplitude of the phase current; m is the modulation index; φ is the motor input power-factor angle.

Coefficients K_1, K_2, K_3, and K_4 are expressed as follows:

$$\begin{cases} K_1 = \dfrac{1}{2\pi}(V_{d0} + V_{s0}) + \dfrac{k f_{sw} V_{CE}}{\pi} \\ K_2 = \dfrac{1}{8}(R_{ce} + R_{ak}) \\ K_3 = \dfrac{1}{2}(V_{d0} - V_{s0}) \\ K_4 = R_{ce} - R_{ak} \end{cases} \tag{9}$$

where V_{d0} and V_{s0} are the zero-current conduction voltages of the IGBT and the diode, respectively.

As discussed in [26] and [27], the last two terms are negligible. Hence, the inverter loss can be written as follows:

$$P_{loss\_inv} = 6\left(K_1 I_{peak} + K_2 I_{peak}^2\right) \tag{10}$$

The amplitude of the phase current can be expressed by the d- and q-axis currents i_d and i_q, respectively, as follows:

$$I_{peak} = \frac{2}{3}\sqrt{i_d^2 + i_q^2} \tag{11}$$

Based on the equivalent circuit model of the PMSM, the d-axis and q-axis currents (i_d and i_q, respectively) are related to the output torque T_e. Therefore, the power loss of the inverter, P_{loss_inv} is a function of T_e, as follows:

$$P_{loss\_inv} = P_{loss\_inv}(T_e) \tag{12}$$

C. BATTERY LOSS MODEL

A battery is typically represented as a circuit composed of voltage power sources, resistances, and capacitors. A battery model is structured based on the intended function, and examples include the internal resistance, Thevenin, higher-order RC, and PNGV models. The internal resistance model was used in this study (Fig. 5), as the focus was on energy loss instead of the dynamic performance of the battery [27].

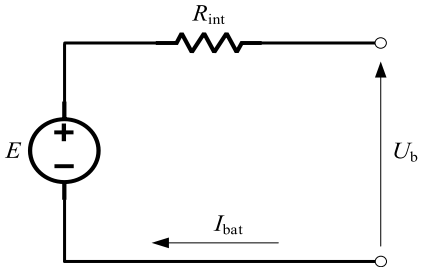

FIGURE 5. Equivalent circuit of battery.

According to Kirchhoff's voltage law, we have

$$E_{batt} = U_b + I_{batt}R_{int} \tag{13}$$

The terminal voltage U_b can be expressed as

$$U_b = \frac{P_{bat\_out}}{I_{batt}} \tag{14}$$

where P_{bat_out} is the output power in the terminal of the equivalent circuit.

From (12) and (13) a quadratic equation in I_{batt} can be derived, written as

$$R_{int}I_{batt}^2 - E_{batt}I_{batt} + P_{bat\_out} = 0 \tag{15}$$

Solve this equation and according to Joule's law in resistance circuit, the power loss in the battery can be expressed as [27]

$$P_{loss\_bat} = \frac{\left(E_{batt} - \sqrt{E_{batt}^2 - 4R_{int}P_{bat\_out}}\right)^2}{4R_{int}} \tag{16}$$

Considering the power loss in the inverter and electric motor, the output power in the terminal of battery P_{bat_out} can be expressed as follows:

$$P_{bat\_out} = T_m\omega_m + P_{loss\_inv} + P_{loss\_mtr} \tag{17}$$

Because the power loss of the inverter, P_{loss_inv}, is a function of T_m (18), and the power loss of the PMSM is a function of (T_m, ω_m) (11), the power loss in the battery, P_{loss_bat}, is a function of T_m and ω_m.

$$P_{loss\_bat} = P_{loss\_bat}(T_m, \omega_m) \tag{18}$$

The power loss of the entire electric subsystem is equal to the sum of the power losses of the electric motor, inverter, and battery.

$$P_{loss\_elec} = P_{loss\_mtr} + P_{loss\_inv} + P_{loss\_bat} \tag{19}$$

D. HYDRAULIC PUMP/MOTOR LOSS MODEL

When the hydraulic system is operating, the liquid flow will not exactly equal the calculated value owing to liquid leakage and compressibility. Volumetric loss refers to power loss caused by oil leakage and compressibility in a hydraulic pump/motor, while another possible source of energy loss in a hydraulic pump/motor is friction between the moving components used in its construction. This type of power loss is known as mechanical loss, which causes the output torque to be less than its theoretical value. Consequently, hydraulic pump/power motor losses can be classified into volumetric and mechanical losses. The expressions of the loss model proposed by Grandall were used in this study [28], [29].

The volumetric loss of the pump is expressed as follows:

$$\Delta q_{pump} = C_s^* D_{pump}\left(\frac{p_{out}}{\mu}\right) + \omega_{pump}D_{pump}\left(\frac{p_{out}}{B}\right)\left(V_r + \frac{1+x}{2}\right) \tag{20}$$

Meanwhile, the torque loss can be expressed as follows:

$$\Delta T_{pump} = C_v^*\mu\omega_{pump}D_{pump} + C_f^* p_{out}D_{pump} \tag{21}$$

where μ and B are oil property parameters. Here, μ is the absolute viscosity of the oil, and B is the fluid bulk modulus; pout is the pressure difference between the inlet and outlet of the pump; ω is the rotational speed of the pump; D_{pump} denotes the maximum pump displacement; V_r is the ratio of the clearance volume to the swept volume; X is the fractional displacement (0–1).

In the formulas for volumetric and mechanical losses, C_s^*, C_v^*, and C_f^* represent the leakage coefficient, viscous friction coefficient, and Coulomb friction coefficient, respectively, expressed as follows:

$$\begin{aligned} C_s^* &= C_s\left(\frac{p_{out}}{p_{atm}}\right)\left(k_{s1} + k_{s2}\frac{\omega_{pump}}{\omega_{max}}\right) \\ C_v^* &= C_v\left(k_{v1} + k_{v2}X\right) \\ C_f^* &= C_f\left(k_{f1} + k_{f2}\frac{\omega_{pump}}{\omega_{max}} + k_{f3}\frac{\omega_{pump}}{\omega_{max}}\right)\left(k_{f4} + k_{f5}X\right) \end{aligned} \tag{22}$$

These coefficients are presented as functions of the rotational speed in Dorey's model instead of constants, which resulted in a better agreement with the experimental results. In the expressions, the coefficients C_s, C_v, and C_f are constants, whereas k_{s1}, k_{s2}, k_{v1}, k_{v2}, k_{f1}, k_{f2}, k_{f3}, k_{f4}, and k_{f5} are polynomial coefficients determined via least-squares fitting.

Equation (24) shows the relationship between the torque loss and the pressure difference at the pump outlet. Because the power loss of the hydraulic system is expressed as a function of pressure and flow rate, the torque loss must be converted to a pressure loss.

The outlet pressure is expressed as follows:

$$p_{out} = \frac{2\pi\left(T_{pump} - C_v^*\mu\omega_{pump}D/60\cdot 10^6\right)}{DX + C_f^*D} \tag{23}$$

The ideal pressure (disregarding the torque loss) of the pump outlet is expressed as follows:

$$p_{ideal} = \frac{2\pi T_{pump}}{D_{pump}X} \tag{24}$$

The difference between these two pressures is the pressure loss of the pump, which is expressed as follows:

$$\Delta p_{pump} = p_{out} - p_{ideal} \tag{25}$$

E. POWER LOSS MODEL OF HYDRAULIC VALVE AND PIPE

Pressure loss occurs in the hydraulic circuit when oil flows through elbows, joints, and sudden-change sections and is regarded as local pressure loss in the hydraulic circuit. This type of pressure loss can also occur in hydraulic valves. However, owing to the viscosity of the liquid, the pressure decreased as the oil flowed through the pipeline. Because both types of pressure loss are proportional to the fluid kinetic energy, the losses of the hydraulic pipeline and valves can be expressed as follows:

$$\Delta p_{\mathrm{pv}} = \xi \frac{\rho v_{\mathrm{oil}}^2}{2} \tag{26}$$

where ξ is the resistance coefficient of the hydraulic pipe and valve, and v_{oil} is the average flow velocity of the hydraulic oil.

The pressure loss of the hydraulic system is expressed as

$$\Delta p_{\mathrm{hyd}} = \Delta p_{\mathrm{pv}} + \Delta p_{\mathrm{pump}} \tag{27}$$

The power loss of the hydraulic system can be expressed as a function of the pressure difference Δp_{hyd} and oil flow rate q as follows:

$$\begin{aligned} P_{\mathrm{loss\_hyd}} &= p_{\mathrm{ideal}} q_{\mathrm{ideal}} - \left(p_{\mathrm{ideal}} - \Delta p_{\mathrm{hyd}}\right)\left(q_{\mathrm{ideal}} - \Delta q_{\mathrm{pump}}\right) \\ &= p_{\mathrm{ideal}} \Delta q_{\mathrm{pump}} + q_{\mathrm{ideal}} \Delta p_{\mathrm{hyd}} - \Delta p_{\mathrm{hyd}} \Delta q_{\mathrm{pump}} \end{aligned} \tag{28}$$

Equations (30)–(32) show that the pressure loss of the hydraulic pump is a function of the output torque T_{pump} and the rotational speed ω_{pump}. Similarly, (26) and (30) show that the oil flow loss is a function of T_{pump} and ω_{pump}. Based on this fact, and (35), the power loss of the hydraulic system, $P_{\mathrm{loss\_hyd}}$, is a function of T_{pump} and ω_{pump} as follows:

$$P_{\mathrm{loss\_hyd}} = P_{\mathrm{loss\_hyd}}\left(T_{\mathrm{pump}}, \omega_{\mathrm{pump}}\right) \tag{29}$$

F. POWER DISSIPATED IN THE FRICTIONAL BRAKING SYSTEM

A frictional braking system is essential for the entire braking system, to ensure safety and adaptability. The energy transferred to the frictional braking system is dissipated into the air as heat, which implies that the power loss of the frictional braking system can be expressed as follows:

$$P_{\mathrm{loss\_fric}} = F_{\mathrm{fric}} v_{\mathrm{brk}} \tag{30}$$

where F_{fric} is the braking force generated by the frictional braking system, N, and v_{brk} is the velocity of the vehicle (m/s).

G. PARAMETERS USED IN MODELS

Several different parameters are used in the mathematical models of the components, such as the copper and iron resistances of the electric motors, d-axis and q-axis inductances of the electric motors, and coefficients in the hydraulic torque and flow loss models. These parameter values were all derived from experimental data.

The measured efficiency map cannot be used directly because it was measured using the MPTA control method, which differs from the LMC method. Because the current distribution based on the MPTA control method was determined in advance, the parameters in the motor's equivalent circuit model can be calculated using data fitting methods. Table 2 lists the parameters of the electric motors.

TABLE 2. Parameters of the electric motors.

Parameters	Front motor	Rear motor
L_{d} (mH)	0.53	1.86
L_{q}(mH)	1.08	4.5
R_{s}(Ω)	0.118	0.418
R_{c}(Ω)	303.5	769.3
ψ_{f}(Wb)	0.199	0.505

Fig. 6 shows the model-calculated efficiency maps of the electric motors compared with the experimental efficiency data.

IV. BRAKING TORQUE DISTRIBUTION BASED ON MINIMUM ENERGY LOSS

As mentioned previously, the DMEHH powertrain contains three distinct energy conversion devices; a front motor with rated power of 30 kW, a rear motor with rated power of 50 kW, and a hydraulic pump. As these components have different efficiency characteristics, the total energy loss of the system is determined by the distribution of the required torque in these devices during braking. Because the primary goal of the control strategy for the DMEHH regenerative braking system is to recover the maximum amount of kinetic energy, a braking torque distribution strategy based on minimum energy loss must be developed. Another assumption that the tire-road adhesion condition is sufficient is set to avoid braking stability issues which will be discussed in future works by the authors.

Assuming that the vehicle must be braked at a certain deceleration based on the initial speed, the required braking deceleration can be converted into the braking force F_{b}. The required braking force was assigned to the front and rear axles at a ratio of β_1, which is known as the primary distribution coefficient. The front regenerative braking force can be categorized into those forces generated by the hydraulic and electric systems at a ratio of β_2 (secondary distribution coefficient). Here, β_1 and β_2 are expressed as follows:

$$\begin{cases} \beta_1 = {F_{\mathrm{f}}}/{F_{\mathrm{b}}} \\ \beta_2 = {F_{\mathrm{mtr\_f}}}/{F_{\mathrm{f}}} \end{cases} \tag{31}$$

where F_{f} is the front braking force and F_{hyd} is the hydraulic braking force on the front axle.

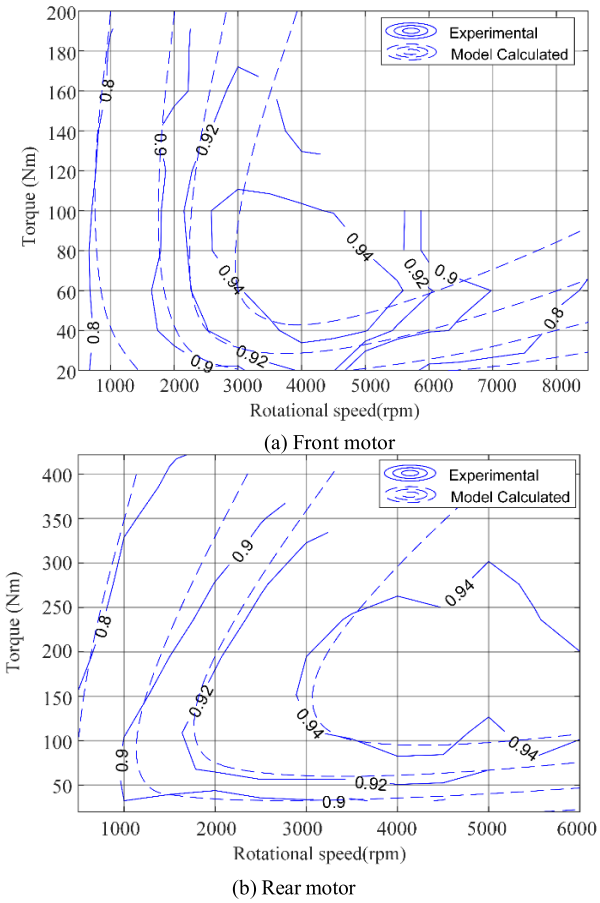

FIGURE 6. Comparison between experimental and model calculated values.

Equation (14) shows that the power loss of the electric system is a function of the output torque and the rotational speed of the electric motor, whereas (24) shows that the power loss of the hydraulic subsystem is a function of the output torque and the rotational speed of the hydraulic pump. The total powertrain power loss is the sum of the power losses of the subsystems as follows:

$$P_{\text{loss\_total}} = P_{\text{loss\_elec}} + P_{\text{loss\_hyd}} + P_{\text{loss\_fric}} \tag{32}$$

Using the transmission ratio of the final drive, the required forces can be converted to the torques required by different energy conversion elements (T_{pump}, $T_{\text{m\_f}}$, and $T_{\text{m\_r}}$), whereas the vehicle speed can be converted into the associated rotational speeds (ω_{pump}, $\omega_{\text{m\_f}}$, and $\omega_{\text{m\_f}}$). The power loss of the entire powertrain system can be calculated by substituting the torque and speed values into the power loss calculation functions. Therefore, the power loss of the entire system can be expressed as a function of the required braking force F_{b}, vehicle velocity v_{brk}, and distribution coefficients β_1 and β_2, as follows:

$$P_{\text{loss\_total}} = P_{\text{loss\_total}}\left(F_{\text{b}}, v_{\text{brk}}\left(t\right), \beta_1, \beta_2\right) \tag{33}$$

Subsequently, the energy loss in the complete braking process, $E_{\text{loss\_brk}}$, can be calculated using the power integral over the time range in the braking process as follows:

$$E_{\text{loss\_total}} = \int_0^{t_{brk}} P_{\text{loss\_total}}\left(F_{\text{b}}, v_{\text{brk}}\left(t\right), \beta_1, \beta_2\right) dt \tag{34}$$

which is a function of F_{b}, β_1, and β_2. Here, t_{brk} is the braking time when the braking force is F_{b}.

The goal of this study is to minimize energy loss during the braking process. Therefore, the energy loss minimization (ELM) optimization problem is expressed as follows:

$$\begin{aligned} &\textit{minimize } E_{\text{loss\_total}}\left(F_{\text{b}}, \beta_1, \beta_2\right) \\ &\textit{subject to } F_{\text{b}} \cdot \beta_1 \cdot \beta_2 \cdot i_{g1} \le T^{\text{f}}_{\text{mtr\_max}} \\ &\qquad F_{\text{b}} \cdot \left(1-\beta_1\right) \cdot i_{g2} \le T^{\text{r}}_{\text{mtr\_max}} \\ &\qquad F_{\text{b}} \cdot \beta_1 \cdot \left(1-\beta_2\right) \cdot i_{g1} \le T_{\text{pump\_max}} \\ &\qquad \left(F_{\text{b}}\beta_1, F_{\text{b}}\left(1-\beta_1\right)\right) \in \mathbf{F}_{ECE} \end{aligned} \tag{35}$$

The first three constraints imply that the command braking torque applied to the motors and the hydraulic pump cannot exceed their limits. The final constraint condition requires that the brake force distributed between the front and rear axles satisfy the ECE R13 regulation, which is detailed in [30].

Solving (35) analytically is difficult; hence, a numerical method was used to obtain the copper and iron power loss equivalent currents in the d-axis and q-axis. For a required braking force F_{b} and an initial braking velocity, $v_{\text{b\_init}}$, the torque distribution coefficients (β_1 and β_2) can be determined as follows:

(1) Discretize the primary distribution coefficient β_1 in the range of 0 to 1 at a certain step size. The primary distribution set can be written as follows:

$$B_1 = \left\{\beta_1\left(1\right), \beta_1\left(2\right), \cdots, \beta_1\left(i\right), \cdots, \beta_1\left(n_1\right)\right\} \tag{36}$$

where n_1 is the step number of the discretized set of β_1, i indicates an arbitrary index of the discretized set, and

$$\beta_1\left(i\right) = \frac{i}{n_1}\beta_1 \tag{37}$$

(2) Discretize the secondary distribution coefficient $\beta 2$ in the range of 0 to 1 for a certain step size. The secondary distribution set can be written as:

$$B_2 = \left\{\beta_2\left(1\right), \beta_2\left(2\right), \cdots, \beta_2\left(j\right), \cdots, \beta_2\left(n_2\right)\right\} \tag{38}$$

where n_2 is the step number of the discretized set of β_2, j indicates an arbitrary index of the discretized set, and

$$\beta_2\left(j\right) = \frac{j}{n_2}\beta_2 \tag{39}$$

(3) One discretized value of β_1 in B_1 ($\beta_1(i)$) and one discretized value of β_2 in B_2 ($\beta_2(j)$) are then selected. Therefore, the values of the brake torque of the power components can be obtained as follows:

$$\begin{cases} T^{\text{f}}_{\text{mtr}} = \min\left(T^{\text{f}}_{\text{mtr\_max}}, \beta_1(i)\left[1-\beta_2(j)\right]F_{\text{b}}i_{g1}\right) \\ T^{\text{r}}_{\text{mtr}} = \min\left(T^{\text{r}}_{\text{mtr\_max}}, \left[1-\beta_1(i)\right]\beta_2(j)F_{\text{b}}i_{g2}\right) \\ T_{\text{hyd}} = \min\left(T_{\text{pump\_max}}, \beta_1(i)\beta_2(j)F_{\text{b}}i_{g1}\right) \end{cases} \tag{40}$$

(4) Considering the wheel radius and reduction ratio of the final drives in the front and rear axles, the rotational speed of the power components can be expressed as follows:

$$\begin{cases} \omega^{\mathrm{f}}_{\mathrm{mtr}}(t) = \dfrac{i_{\mathrm{g1}} v_{\mathrm{brk}}(t)}{r_{\mathrm{wheel}}} \\ \omega^{\mathrm{r}}_{\mathrm{mtr}}(t) = \dfrac{i_{\mathrm{g2}} v_{\mathrm{brk}}(t)}{r_{\mathrm{wheel}}} \\ \omega_{\mathrm{hyd}}(t) = \dfrac{i_{\mathrm{g1}} v_{\mathrm{brk}}(t)}{r_{\mathrm{wheel}}} \end{cases} \tag{41}$$

The function from $v_{\mathrm{brk}}(t)$ implies that the vehicle speed during the braking process is a function of time. Meanwhile, $v_{\mathrm{brk}}(t)$ is expressed as a function of the required braking force F_{b} and the initial braking speed $v_{\mathrm{brk\_init}}$ as follows:

$$v_{\mathrm{brk}}(t) = v_{\mathrm{brk\_init}} - \frac{F_{\mathrm{b}}}{m_{\mathrm{cargo}}} t \tag{42}$$

(5) Substitute the torque rotational speed values into (4), (10), (13), and (14). Consequently, the power losses of the front and rear electric power subsystems are written as follows (annotated by superscripts f and r):

$$\begin{aligned} P^{f/r}_{\mathrm{loss\_elec}}(i,j) = {} & P_{\mathrm{loss\_mtr}}\left(T^{\mathrm{f/r}}_{\mathrm{mtr}}, \omega^{\mathrm{f/r}}_{\mathrm{mtr}}(t)\right) \\ & + P_{\mathrm{loss\_inv}}\left(T^{\mathrm{f/r}}_{\mathrm{mtr}}\right) \\ & + P_{\mathrm{loss\_batt}}\left(T^{\mathrm{f/r}}_{\mathrm{mtr}}, \omega^{\mathrm{f/r}}_{\mathrm{mtr}}(t)\right) \end{aligned} \tag{43}$$

whereas the power loss of the hydraulic system is expressed as follows based on (24):

$$P_{\mathrm{loss\_hyd}}(i,j) = P_{\mathrm{loss\_hyd}}\left(T_{\mathrm{hyd}}, \omega_{\mathrm{hyd}}(t)\right) \tag{44}$$

Subsequently, based on (25), the power loss of the frictional system can be expressed as follows:

$$P_{\mathrm{loss\_fric}}(i,j) = \left[F_{\mathrm{b}} - \frac{\left(T^{\mathrm{f}}_{\mathrm{mtr}} + T_{\mathrm{hyd}}\right) i_{g1}}{r_{\mathrm{wheel}}} - \frac{T^{\mathrm{r}}_{\mathrm{mtr}} i_{g1}}{r_{\mathrm{wheel}}}\right] v_{\mathrm{brk}}(t) \tag{45}$$

Hence, the total power loss of the entire powertrain during the braking process based on the primary and secondary distribution coefficients, $\beta_1(i)$ and $\beta_2(j)$, is written as follows:

$$\begin{aligned} P_{\mathrm{loss\_total}} = {} & P^{f}_{\mathrm{loss\_elec}}(i,j) + P^{r}_{\mathrm{loss\_elec}}(i,j) \\ & + P_{\mathrm{hyd}}(i,j) + P^{\mathrm{fric}}_{\mathrm{loss}}(i,j) \end{aligned} \tag{46}$$

(6) The energy loss is obtained by integrating the total power loss with respect to time.

$$E_{\mathrm{loss\_total}}(i,j) = \int_0^{t_{end}} P_{\mathrm{loss\_total}}(i,j)\, dt \tag{47}$$

(9) $\beta_1(i') \in B_1$ and $\beta_2(j') \in B_2$ are used, which differs from $\beta_1(i)$ and $\beta_2(j)$, such that another energy loss value $E_{loss\_total}(i', j')$ can be calculated by repeating steps (1)–(6). By considering all the elements in sets B_1 and B_2, an energy-loss set E_{LOSS}, whose element number is $n_1 n_2$, can be generated. The elements of E_{LOSS} are arranged in a matrix with i indexing row elements and j indexing column elements. The matrix form of E_{LOSS} can be written as follows:

$$E_{\mathrm{LOSS}} = \begin{bmatrix} E(1,1) & \cdots & E(1,j) & \cdots & E(1,n_2) \\ \vdots & \ddots & & & \vdots \\ E(i,1) & & E(i,j) & & \vdots \\ \vdots & & & \ddots & \vdots \\ E(n_1,1) & \cdots & \cdots & \cdots & E(n_1,n_2) \end{bmatrix} \tag{48}$$

(10) Obtain the minimum value in the set E_{LOSS}, denoted as $E_{\mathrm{loss\_total}}(\hat{i}, \hat{j})$. The corresponding $\beta_1(\hat{i})$ and $\beta_1(\hat{j})$ are the torque distribution coefficients that minimize energy loss.

The method for determining the ELM torque-distribution coefficients is shown in the diagram below (Fig. 7).

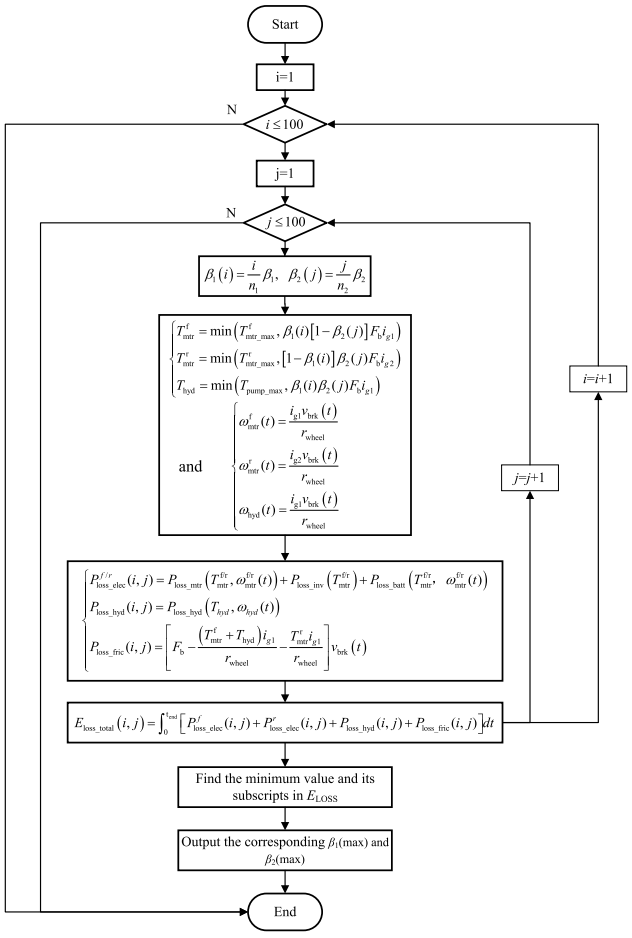

FIGURE 7. Energy loss calculation algorithm.

The ELM torque distribution coefficients of the hybrid braking system for a specified braking force and initial vehicle speed can be obtained by completing the procedure shown in Fig. 7. The energy losses under each different torque distribution scheme were calculated using β_1 and β_2 ranging from 0% to 100%. In all of these schemes, the torque distribution scheme that minimizes energy loss can be selected as the

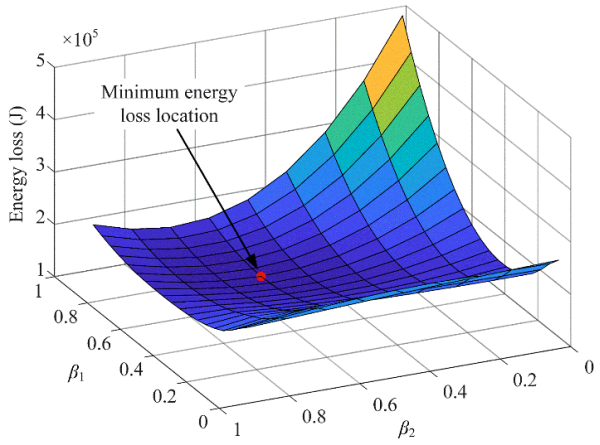

FIGURE 8. Energy losses for various torque distributions (z = 0.4 and u_{init} = 100 km/h).

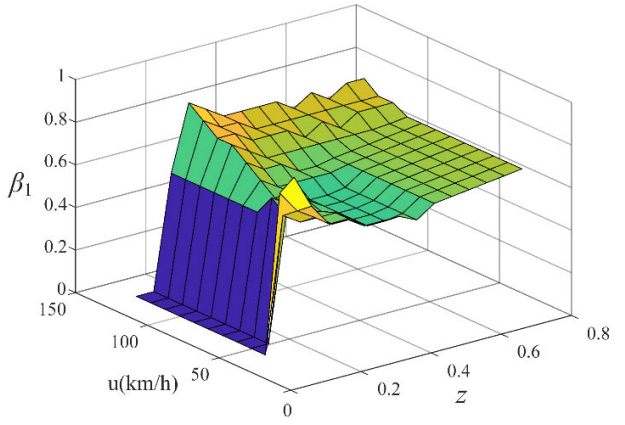

(a) Primary torque distribution map.

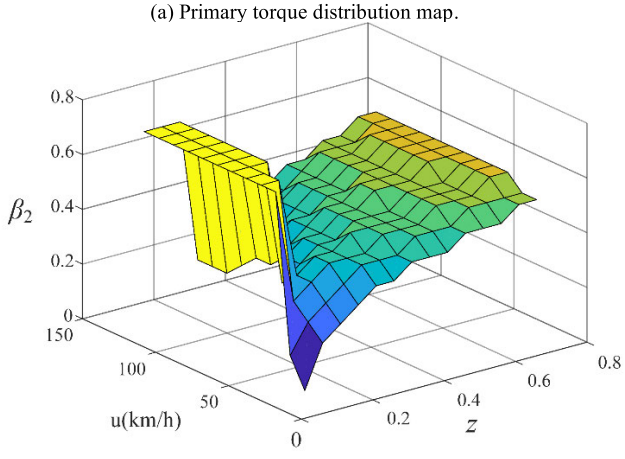

(b) Secondary torque distribution map.

FIGURE 9. Torque distribution coefficient maps.

torque distribution coefficient values for the specified braking force and initial vehicle speed. Fig. 8 shows the energy losses under the conditions of $z = 0.4$ and $u_{init} = 100$ km/h. The red circle denotes the point of minimum energy loss, and its horizontal coordinates are the ELM torque distribution coefficients.

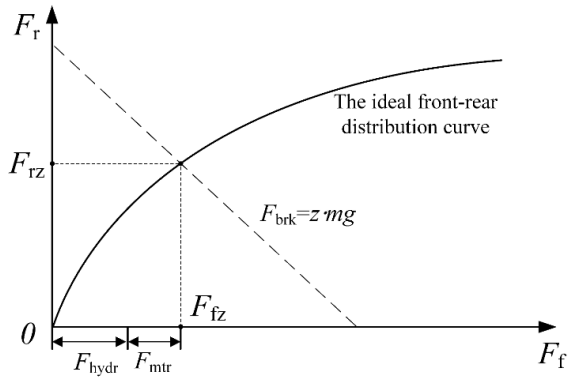

FIGURE 10. Torque distribution under ideal front-rear distribution curve.

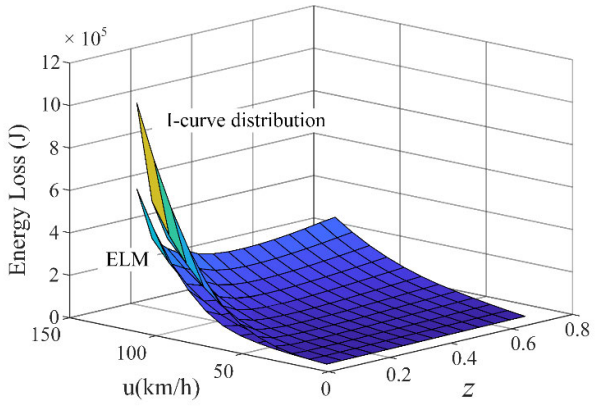

FIGURE 11. Energy loss comparison.

Fig. 9 shows the torque distribution scheme that minimizes the energy loss of the entire powertrain when different braking conditions are considered (different initial speeds and required braking decelerations). The continuous variables (braking deceleration and initial speed) were discretized to form a two-dimensional grid as the calculation program was executed on a computer. To create a map, the torque-distribution schemes at each point on the grid were calculated, and this interpolation method is suitable for practical applications.

Fig. 9 shows sudden changes of β_1 and β_2 when the braking strength z (z=a/g) varies. The value of β_1 is tiny while the value of β_2 is relatively higher when z is less than 0.1. This implies that the rear electric motor plays a major role in low- deceleration braking conditions. The value of β_1 is relatively lower when z is in medium value as well as initial speed is medium and low values, which means a higher proportion of the torque generated by the rear electric motor. Fig. 9 (b) shows an increasing trend when the braking strength z increases (when z>0.1), which indicates that the proportion of the hydraulic-generated braking torque is positively related to brake deceleration. Fig. 9 (b) also shows that β_2 is slightly lower in the low initial speed area, which implies that the energy efficiency is lower compared with the electric motor.

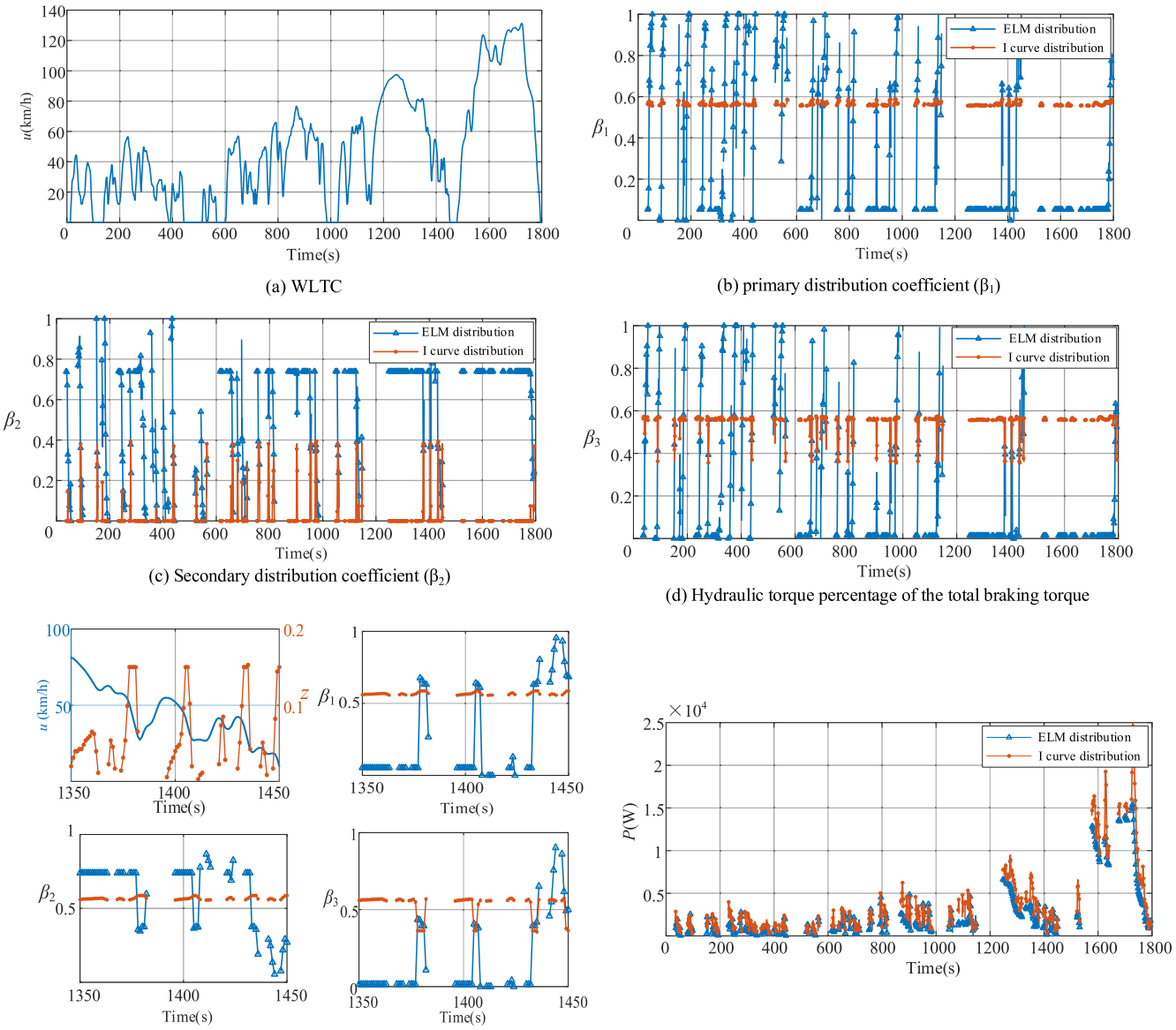

(a) WLTC

(b) primary distribution coefficient (β_1)

(c) Secondary distribution coefficient (β_2)

(d) Hydraulic torque percentage of the total braking torque

(e) Distribution coefficients in the time period 1350—1450s

(f) Power loss

FIGURE 12. Distribution coefficients and power loss in WLTCs.

V. RESULT ANALYSIS

The ideal distribution is a typical braking force distribution between the front and rear axles of passenger cars [6]. In this scheme, the front-rear braking distribution adheres to the ideal front-rear braking force distribution rule, which states that the front-to-rear braking force ratio is equal to the vertical loads on the front and rear axles. The ideal front-rear distribution curve is called the I-curve.

Hydraulic energy storage systems are used to ease the charge and discharge current stress in electric hydraulic hybrid systems [19]. The charge or discharge power is larger at the beginning of the braking or start-up processes. Therefore, the ''hydraulic priorly'' strategy is used in the common torque distribution methods.

The general I-curve primary distribution and hydraulic prior secondary torque distribution scheme were proposed for comparison to demonstrate the advantages of the ELM torque distribution method. The torque distribution strategy in the front axle is based on the rule that the hydraulic pump provides the required braking torque, while the electric motor functions when the torque provided by the hydraulic pump is insufficient. In the following sections, this distribution scheme is referred to as the I-curve distribution scheme. A diagram of the torque distribution is shown in Fig. 10.

The I-curve distribution should be considered to achieve the best utilization of adhesion between tire and road. The energy losses during the entire braking process were calculated for the ELM-based braking torque and I-curve torque distributions as shown in Fig. 11. In general, the energy loss in the minimum energy loss braking torque distribution is less than that in the I-curve torque distribution, particularly at a high initial speed, while under intermediate braking

deceleration and at a low initial speed, the energy losses are similar.

Because the energy losses are lower under any condition (initial speed and braking deceleration), the braking torque distribution, based on the minimum energy loss, can be applied in drive cycles to achieve more efficient energy recovery. In this study, the world light vehicle test cycle (WLTC, as shown in Fig. 12 (a)) was used as the driving cycle. As the focus of this study, braking conditions were obtained. The primary torque distribution coefficient β_1 and secondary distribution coefficient β_2 during braking in the WLTC are shown in Fig. 12(b) and 12(c), respectively. The figures show the total differences between the ELM torque and the I-curve torque distributions. To more clearly show the proportion of the hydraulic torque, the overall percentage of the hydraulic torque to the total regenerative braking torque β_3 is shown in Fig.12(d). β_3 has the calculation equation of $\beta_3 = \beta_1(1-\beta_2)$.

To identify the results more clearly, the local segments of the torque distribution plots, the hydraulic proportion plot, as well as the vehicle's speed and braking deceleration plots, in the time from 1350 to 1450th second are plotted individually and shown in Fig.12(e). As is shown in Fig.12 (e), the torque distribution coefficients vary slightly when the I curve distribution is adopted. When the ELM distribution is employed, the torque distribution coefficients keep unchanged and the overall proportion of the hydraulic torque is close to zero when the braking strength z is less than 0.1. This implies that the efficiency of the hydraulic pump is lower than the electric motors in low output torque, resulting in the dominant role of the electric regenerative systems in this condition. The torque distribution coefficients change largely and the overall proportion of the hydraulic torque varies between 0—1 when the braking strength z is higher. This implies higher participation of the hydraulic system when the required braking torque is higher and demonstrated the effectiveness of the energy loss minimization torque distribution.

Fig. 12(f) shows the power loss difference between the two torque distributions. Fig. 12(f) shows a higher power loss in the I-curve torque distribution, particularly under high-speed conditions. By integrating the power loss over the time range of the WLTC, the total energy loss of the ELM torque distribution was 2.09×10^3 kJ, which is lower than the energy loss of the I-curve torque distribution (2.86×10^3 kJ). Therefore, the energy loss decreased by 27.2%.

TABLE 3. Energy loss comparison in braking process in different driving cycles.

Drive cycle	I-curve distribution	ELM	Energy loss decrease
WLTC	2.86×10^3 kJ	2.09×10^3 kJ	27.2%
UDDS	9.86×10^2 kJ	7.00×10^2 kJ	29.1%
NEDC	5.20×10^2 kJ	3.87×10^2 kJ	25.5%
US06	2.24×10^3 kJ	1.75×10^3 kJ	21.6%

The energy losses in these two torque distribution strategies (ELM and I-curve) during the braking energy recovery process in other typical driving cycles (UDDS, NEDC, and US06) were calculated, and the results are listed in Table 3 along with those in the WLTCs. The energy losses decreased by 27.2, 29.1, 25.5, and 21.6% in the WLTC, UDDS, NEDC, and US06 drive cycles, respectively. The results validated the energy-saving effect of the ELM torque-distribution strategy.

VI. CONCLUSION

Based on the DMEHH powertrain, a braking torque distribution method based on minimum energy loss with an electric motor controlled via LMC was devised in this study.

The DMEHH powertrain comprises a single electric-motor-driven rear axle and a hydraulic-electric-hybrid-driven front axle. The front-rear system operates individually via an electric motor and offers control and flexibility in both driving and braking modes, which could improve the utilization rate of electric motors. A hydraulic energy storage system was incorporated to provide a high-power output when the vehicle was required to accelerate or absorb a high-power input in the initial stage of the braking mode, as the utilization of a hydraulic energy storage system can reduce the current load to the battery, thereby effectively extending its service life.

The incorporation of a hydraulic energy storage system increases the complexity of the system, resulting in a demand for energy management. To establish a control strategy for the DMEHH powertrain, power loss models of the hydraulic and electric subsystems were established based on the different characteristics of the power conversion components (electric motor and hydraulic pump/motor), energy transferring components (power inverter and hydraulic valves and pipes), and energy storage components (battery) in the corresponding subsystems. The control algorithm of the PMSM used the LMC method other than the previous works which used the numerical efficiency maps [8] Several practical tests were conducted to obtain the key parameters and coefficients to obtain the main parameters of the models.

Subsequently, a torque distribution method based on minimum energy loss was devised, and by performing the minimal energy loss calculation for all braking conditions (initial speed and braking deceleration), the primary and secondary torque distribution coefficient maps were obtained. When these coefficient maps were applied in the ELM torque distribution strategy, the energy loss of the powertrain under any braking condition remained minimal compared with the conventional I-curve torque distribution scheme. The energy losses when braking for different driving cycles were calculated by comparing the ELM and general I-curve torque distribution strategies. The energy losses during the braking energy recovery process decreased by 27.2% in the WLTC, 29.1% in the UDDS, 25.5% in the NEDC, and 21.6% in the US06, which demonstrates the significant effect of the ELM braking torque distribution strategy.

REFERENCES

[1] M. S. Kumar and S. T. Revankar, "Development scheme and key technology of an electric vehicle: An overview," *Renew. Sustain. Energy Rev.*, vol. 70, pp. 1266–1285, Apr. 2017, doi: 10.1016/j.rser.2016.12.027.

[2] S. S. Williamson, *Energy Management Strategies for Electric and Plug-in Hybrid Electric Vehicles*. New York, NY, USA: Springer, 2013.
[3] S. Umans, A. Fitzgerald, C. Kingsley, *Electric Machinery*. New York, NY, USA: McGraw-Hill, 2013.
[4] H. Zhang, W. Chen, Z. Shang, Z. Xu, Z. Gao, Y. Chen, and H. Ren, "Optimum driving system design for dual-motor pure electric vehicles," *J. Beijing Inst. Technol.*, vol. 29, no. 4, pp. 592–602, Dec. 2020, doi: 10.15918/j.jbit1004-0579.20079.
[5] X. Hu, Y. Li, C. Lv, and Y. Liu, "Optimal energy management and sizing of a dual motor-driven electric powertrain," *IEEE Trans. Power Electron.*, vol. 34, no. 8, pp. 7489–7501, Aug. 2019, doi: 10.1109/TPEL.2018.2879225.
[6] Y. Gao, L. Chen, and E. Mehrdad, "Investigation of the effectiveness of regenerative braking for EV and HEV," *SAE Trans.*, vol. 108, pp. 3184–3190, Jan. 1999, Accessed: Jun. 20, 2022. [Online]. Available: http://www.jstor.org/stable/44733986
[7] Z. Ma and D. Sun, "Energy recovery strategy based on ideal braking force distribution for regenerative braking system of a four-wheel drive electric vehicle," *IEEE Access*, vol. 8, pp. 136234–136242, 2020, doi: 10.1109/ACCESS.2020.3011563.
[8] J. Kim, "Optimal power distribution of front and rear motors for minimizing energy consumption of 4-wheel-drive electric vehicles," *Int. J. Automot. Technol.*, vol. 17, no. 2, pp. 319–326, Apr. 2016, doi: 10.1109/TPEL.2018.2879225.
[9] X. Yuan and J. Wang, "Torque distribution strategy for a front- and rear-wheel-driven electric vehicle," *IEEE Trans. Veh. Technol.*, vol. 61, no. 8, pp. 3365–3374, Oct. 2012, doi: 10.1109/TVT.2012.2213282.
[10] K. Chang, "Loss minimization control of permanent magnet synchronous machine for electric vehicle applications," M.S. thesis, Dept. Elect. Eng., Concordia Univ., Montreal, QC, Canada, 2013.
[11] N. P. Quang and J. A. Dittrich, *Vector Control of Three-Phase AC Machines*, vol. 2. Berlin, Germany: Springer, 2008.
[12] S. Morimoto, Y. Tong, Y. Takeda, and T. Hirasa, "Loss minimization control of permanent magnet synchronous motor drives," *IEEE Trans. Ind. Electron.*, vol. 41, no. 5, pp. 511–517, Oct. 1994, doi: 10.1109/41.315269.
[13] J. Lee, K. Nam, S. Choi, and S. Kwon, "Loss minimizing control of PMSM with the use of polynomial approximations," in *Proc. IEEE Ind. Appl. Soc. Annu. Meeting*, Oct. 2008, pp. 1–9, doi: 10.1109/08IAS.2008.226.
[14] J. Leon, J. M. Garcia, M. J. Acero, A. Gonzalez, G. Niu, and M. Krishnamurthy, "Case study of an electric-hydraulic hybrid propulsion system for a heavy duty electric vehicle," Society of Automotive Engineers (SAE), Warrendale, PA, USA, SAE Tech. Papers 2016-01-8112, 2016, doi: 10.4271/2016-01-8112.
[15] S. Baseley, C. Ehret, E. Greif, and M. G. Kliffken, "Hydraulic hybrid systems for commercial vehicles," Society of Automotive Engineers (SAE), Warrendale, PA, USA, SAE Tech. Papers 2007-01-4150, 2007, doi: 10.4271/2007-01-4150.
[16] F. Wasbari, R. A. Bakar, L. M. Gan, M. M. Tahir, and A. A. Yusof, "A review of compressed-air hybrid technology in vehicle system," *Renew. Sustain. Energy Rev.*, vol. 67, pp. 935–953, Jan. 2017, doi: 10.1016/j.rser.2016.09.039.
[17] J. Wu, X. Wang, L. Li, C. Qin, and Y. Du, "Hierarchical control strategy with battery aging consideration for hybrid electric vehicle regenerative braking control," *Energy*, vol. 145, no. 1, pp. 301–312, Feb. 2018, doi: 10.1016/j.energy.2017.12.138.
[18] M. Abdel-Monem, K. Trad, N. Omar, O. Hegazy, P. Van Den Bossche, and J. Van Mierlo, "Influence analysis of static and dynamic fast-charging current profiles on ageing performance of commercial lithium-ion batteries," *Energy*, vol. 120, pp. 179–191, Dec. 2017, doi: 10.1016/j.energy.2016.12.110.
[19] G. Niu, F. Shang, M. Krishnamurthy, and J. M. Garcia, "Evaluation and selection of accumulator size in electric-hydraulic hybrid (EH2) powertrain," in *Proc. IEEE Transp. Electrific. Conf. Expo. (ITEC)*, Jun. 2016, pp. 1–6, doi: 10.1109/ITEC.2016.7520255.
[20] Y. Sun, J. Garcia, and M. Krishnamurthy, "A novel fixed displacement electric-hydraulic hybrid (EH2) drivetrain for city vehicles," in *Proc. IEEE Transp. Electrific. Conf. Expo (ITEC)*, Jun. 2013, pp. 1–6, doi: 10.1109/itec.2013.6574499.
[21] R. Ramakrishnan, S. S. Hiremath, and M. Singaperumal, "Design strategy for improving the energy efficiency in series hydraulic/electric synergy system," *Energy*, vol. 67, pp. 422–434, Apr. 2014, doi: 10.1016/j.energy.2014.01.057.
[22] J. J. Eckert, T. P. Barbosa, S. F. Da Silva, F. L. Silva, L. C. A. Silva, and F. G. Dedini, "Electric hydraulic hybrid vehicle powertrain design and optimization-based power distribution control to extend driving range and battery life cycle," *Energy Convers. Manage.*, vol. 252, Jan. 2022, Art. no. 115094, doi: 10.1016/j.enconman.2021.115094.
[23] N. Urasaki, T. Senjyu, and K. Uezato, "An accurate modeling for permanent magnet synchronous motor drives," in *Proc. 15th Annu. IEEE Appl. Power Electron. Conf. Expo.*, Feb. 2000, pp. 387–392, doi: 10.1109/APEC.2000.826132.
[24] Y. Yang, C. Luo, and P. Li, "Regenerative braking control strategy of electric-hydraulic hybrid (EHH) vehicle," *Energies*, vol. 10, no. 7, p. 1038, Jul. 2017, doi: 10.3390/en10071038.
[25] C. Cavallaro, A. O. D. Tommaso, R. Miceli, A. Raciti, G. R. Galluzzo, and M. Trapanese, "Efficiency enhancement of permanent-magnet synchronous motor drives by online loss minimization approaches," *IEEE Trans. Ind. Electron.*, vol. 52, no. 4, pp. 1153–1160, Aug. 2005, doi: 10.1109/TIE.2005.851595.
[26] Y. Yang, Q. He, C. Fu, S. Liao, and P. Tan, "Efficiency improvement of permanent magnet synchronous motor for electric vehicles," *Energy*, vol. 213, Dec. 2020, Art. no. 118859, doi: 10.1016/j.energy.2020.118859.
[27] D. Lu, M. Ouyang, J. Gu, and J. Li, "Optimal velocity control for a battery electric vehicle driven by permanent magnet synchronous motors," *Math. Problems Eng.*, vol. 2014, pp. 1–14, Jan. 2014, doi: 10.1155/2014/193960.
[28] D. McCandlish and R. E. Dorey, "The mathematical modelling of hydrostatic pumps and motors," *Proc. Inst. Mech. Eng., B, Manage. Eng. Manuf.*, vol. 198, no. 3, pp. 165–174, Aug. 1984, doi: 10.1243/pime_proc_1984_198_062_02.
[29] D. R. Grandall, "The performance and efficiency of hydraulic pumps and motors," M.S. thesis, Fac. Graduate School, Univ. Minnesota, Minneapolis, MN, USA, 2010. [Online]. Available: https://hdl.handle.net/11299/59818
[30] *Regulation No 13 of the Economic Commission for Europe of the United Nations (UN/ECE)—Uniform Provisions Concerning the Approval of Vehicles of Categories M, N and O With Regard to Braking [2016/194]*, Official Journal of the European Union, Luxembourg, 2016. [Online]. Available: https://eur-lex.europa.eu/legal-content/EN/TXT/?uri=CELEX:42016X0218(01)

CHANG LUO received the M.S. degree in automotive engineering from Chongqing University, Chongqing, China, in 2016, where he is currently pursuing the Ph.D. degree. His current research interest includes control and dynamics of automotive powertrains.

YANG YANG (Member, IEEE) received the Ph.D. degree in mechanical engineering from Chongqing University, Chongqing, China, in 2008. He is currently a Professor with the College of Mechanical Engineering, Chongqing University. He has authored or coauthored more than 60 academic articles within his academic career. His research interests include dynamics of electromechanical systems and control of braking systems.

ZHEN ZHONG received the M.S. degree in automotive engineering from Chongqing University, Chongqing, China, in 2021. His current research focus on hydraulic drive system of the off-road vehicle.